Catalysis Today 269 (2016) 122–131

Contents lists available at ScienceDirect

Catalysis Today

journal homepage: www.elsevier.com/locate/cattod

Catalytic conversion of sorbitol to gasoline-ranged products without external hydrogen over Pt-modified Ir-ReO_x/SiO_2

Sibao Liu [a], Yasuyo Okuyama [b], Masazumi Tamura [a], Yoshinao Nakagawa [a,*], Akio Imai [b], Keiichi Tomishige [a,*]

[a] Department of Applied Chemistry, School of Engineering, Tohoku University, 6-6-07, Aoba, Aramaki, Aoba-ku, Sendai 980-8579, Japan
[b] Central Research & Development Laboratory, Showa Shell Sekiyu K.K., 4052-2 Nakatsu, Aikawa-cho, Aikoh-gun, Kanagawa-ken, Japan

ARTICLE INFO

Article history:
Received 23 June 2015
Received in revised form 3 October 2015
Accepted 8 October 2015
Available online 11 November 2015

Keywords:
Sorbitol
Gasoline
Aqueous phase reforming
Hydrogenolysis

ABSTRACT

Deoxygenation of sorbitol was carried out over a Pt-modified Ir-ReO_x/SiO_2 catalyst in biphasic solvent system (*n*-decane + H_2O) without external hydrogen. Good yield of gasoline-ranged products was obtained including C5–C6 alkanes and C2–C6 mono-functionalized compounds such as ketones, alcohols, cyclic ethers and carboxylic acids. The Pt(3 wt%)-Ir-ReO_x/SiO_2 catalyst showed the best performance in the production of gasoline-ranged products. The maximum yield of gasoline-ranged products was 42%. The distribution of the products can be tuned by the addition of HZSM-5. The main products were C5–C6 alkanes with addition of HZSM-5 while the main products were C2–C6 mono-functionalized compounds without addition of HZSM-5. Characterizations such as TPR, XRD, TEM, XANES, EXAFS, CO adsorption were performed. The results demonstrated that the Pt-Ir-ReO_x/SiO_2 catalyst showed the structure of Pt-Ir alloy particles partially covered with ReO_x species. The number of surface Pt atoms in Pt(3)-Ir-ReO_x/SiO_2 was larger than that of Pt/SiO_2 or Pt-ReO_x/SiO_2 because of the small size of Pt-Ir alloy particles. The large number of surface Pt atoms and the synergetic effect of Pt, Ir and ReO_x species make the catalyst efficiently generate hydrogen by aqueous phase reforming of sorbitol, and the generated hydrogen is consumed in the hydrogenolysis C—O bonds.

1. Introduction

Decreasing oil supplies, increasing energy demand and global warming issues provide incentives to conversion of renewable biomass into high-quality transportation fuels and valuable chemical feedstocks [1–9]. Recently, particular interest has been attracted on producing gasoline-ranged products by aqueous-phase hydrodeoxygenation of biomass-derived sugars or sugar alcohols, especially sorbitol [10–20]. Several Pt-based catalysts supported on carbon, solid acids, metal oxide and metal oxide phosphates has been reported in the literature as promising catalysts for this process [10–20]. The total yield of gasoline-range products including C5–C6 alkanes and C2–C6 mono-functionalized compounds could reach around 40–70% over these Pt-based catalysts. However, a high pressure of hydrogen was needed for the processes. Considering the high cost of fossil-derived hydrogen and potential safety issues which caused by the high pressure hydrogen, the industrial prospect of this process is becoming a challenge. In 2002, Dumesic et al. reported aqueous phase reforming (APR) of polyols (sorbitol, glycerol and ethylene glycol) to produce hydrogen over Pt-based catalyst at 498 K [21]. Later the same group [22] and the group of Murzin et al. investigated APR of sorbitol and found that some amounts of less-oxygenated organic products such as ≥C4 mono-oxygenates can be formed [23,24]. It seems worthwhile to evaluate the possibility of production of useful less-oxygenated organics using in situ generated hydrogen and catalysts with higher hydrogenolysis activity. A lot of works on the conversion of glycerol to 1,2-propanediol by using this biorefinery concept were reported [25–33]. However, the most abundant sugar alcohol, sorbitol, has unexpectedly attracted very little attention [10,21–24,34]. Sorbitol is a very important biomass-derived platform molecule, which can be produced from cellulose by hydrolysis and hydrogenation [35–37]. Therefore, efficient conversion of sorbitol to gasoline-ranged products in high yield without external hydrogen could be very meaningful.

In our previous work, we have found that Ir-ReO_x/SiO_2 catalyst shows high C—O hydrogenolysis activity and almost no C—C cracking activity [38,39]. However, APR of polyols involves C—C dissociation and thus the catalyst should have some C—C

* Corresponding authors.
E-mail addresses: yoshinao@erec.che.tohoku.ac.jp (Y. Nakagawa), tomi@erec.che.tohoku.ac.jp (K. Tomishige).

http://dx.doi.org/10.1016/j.cattod.2015.10.023
0920-5861/

cracking activity. Therefore, in this study, we modified Ir-ReO_x/SiO_2 with other noble metals, especially Pt, to improve its C—C cracking activity and balance the C—O and C—C dissociation performance to obtain high yield of gasoline-ranged products from sorbitol.

2. Experimental

2.1. Catalyst preparation

The SiO_2 (G-6, BET surface area 535 m^2/g) supplied by Fuji Silysia Chemical Ltd. was used as a support of the catalysts. Before impregnation, SiO_2 was calcined in air at 973 K for 1 h. Ir-ReO_x/SiO_2 catalysts were prepared by sequential impregnation method as described previously [40–48]. First, Ir/SiO_2 was prepared by impregnating with an aqueous solution of H_2IrCl_6 (Furuya Metals Co., Ltd). After evaporating the solvent at ≤353 K and drying at 383 K for 12 h, they were impregnated with an aqueous solution of NH_4ReO_4 (Soekawa Chemical Co., Ltd.). These catalysts were calcined in a crucible in air at 773 K for 3 h after drying at 383 K for 12 h. Then the obtained Ir-ReO_x/SiO_2 catalyst was impregnated with an aqueous solution of H_2PtCl_6 (Soekawa Chemical Co., Ltd.), $RhCl_3$ (Wako Pure Chemical Industries, Ltd.), $PdCl_2$ (Soekawa Chemical Co., Ltd.), or $RuCl_3$ (Strem Chemicals Co., Ltd.). After evaporating the solvent and drying at 383 K for 12 h, they were calcined in air at 773 K for 3 h. The loading amounts of Ir and Re were 4.0 and 7.8 wt%, respectively (Re/Ir molar ratio = 2), and that of additive was represented by the weight percent of the additives to the total catalyst in parenthesis like M(x)-Ir-ReO_x/SiO_2 (M = Pt, Rh, Pd, Ru). All the catalysts were used in powdered form with a granule size of <100 mesh. HZSM-5 [JRC-Z5-90 H(1), Süd-Chemie Catalysts and Catalysis Society of Japan, Si/Al_2 = 90] was used as received.

2.2. Activity tests

Activity tests were performed in a 190-ml stainless steel autoclave with an inserted glass vessel. The catalyst was put into an autoclave together with a spinner and an appropriate amount of water and heated at 473 K with 8 MPa H_2 for 1 h for the reduction pretreatment. The stirring rate was 250 rpm. After the pretreatment, the autoclave was cooled down, and hydrogen was removed. Sorbitol (0.5 g, Wako Pure Chemical Industries, Ltd., 98%) and *n*-decane (20 ml; Tokyo Chemical Industry Co. Ltd., 99%) were put into the autoclave. HZSM-5 was also added when necessary. After sealing the reactor, the air content was purged by flushing three times with Ar (1 MPa, 99.99%; Nippon Peroxide Co., Ltd.). The reactor was pressurized with Ar to 0.5–4.0 MPa at room temperature and then heated to set temperatures (443–473 K). The heating took about 1–1.5 h. After the temperature reached the set one, the temperature was kept for appropriate reaction time. The stirring rate was 500 rpm. After reaction, the reactor was cooled down by using ice bath and the gases were collected in a gas bag. The reaction mixture was separated into organic and aqueous phases. The autoclave contents were transferred to a vial, and the catalyst was separated by centrifugation and filtration.

The products were isosorbide, ketones: 2-hexanone, 3-hexanone, 2-pentanone, 3-pentanone, butanone and actone; mono-alcohols: 1-hexanol, 2-hexanol, 3-hexanol, 1-pentanol, 2-pentanol and 3-pentanol; cyclic ethers: 2-methyltetrahydrofuran, 2,5-dimethyltetrahydrofuran and 2-methyltetrahydropyran; acids: acetic acid, propanoic acid, butanoic acid, valeric acid and hexanoic acid; alkanes: *n*-hexane, 2-methylpentane, 3-methylpentane, *n*-pentane, *n*-butane, propane, ethane and methane; CO_2; H_2 and other products that could not be identified. Sorbitol and isosorbide in the aqueous phase were analyzed by using HPLC (Shimadzu LC-10A) with a refractive index detector (RID) and a Phenomenex Rezex RPM-Monosaccharide Pb + 2 column (diameter 7.8 mm, 300 mm). Ketones, mono-alcohols and acids in the aqueous phase were analyzed by using gas chromatograph (Shimadzu GC-2014) equipped with TC-WAX capillary column (diameter 0.25 mm, 30 m) and FID. Alkanes, ketones, cyclic ethers and mono-alcohols in the organic phase were analyzed by gas chromatograph (Shimadzu GC-2014) equipped with DB-1 capillary column (diameter 0.25 mm, 30 m) and FID. Alkanes in the gas phase were analyzed by gas chromatograph (Shimadzu GC-2014) equipped with an Rtx-1-PONA capillary column (diameter 0.25 mm, 100 m) and FID. CO_2 in the gas phase was analyzed by gas chromatograph (Shimadzu GC-2014) equipped with a Gaskuropack 54 column, a methanator and FID, and H_2 was analyzed by the same GC with MS-13X packed column and TCD.

The conversion of substrate (sorbitol) and the yield of products were calculated on the carbon basis and defined as follows:

$$\text{Conversion [\%C]} = \frac{\text{mol of total C atoms in substrate} - \text{mol of C atoms in unreacted substrate}}{\text{mol of total C atoms in substrate}} \times 100$$

$$\text{Yield of detected products [\%C]} = \frac{\text{mol}_{\text{product}} \times \text{C atoms in product}}{\text{mol of total C atoms in substrate}} \times 100$$

$$\text{Loss of carbon balance [\%C]} = \text{Conversion} \times 100 - \text{the sum of yield of detected products} \times 100$$

The conversion of sorbitol with hydrogen was also conducted with the same method. The pressure of hydrogen was 6 MPa at room temperature. In the case of conversion of glycerol (Wako Pure Chemical Industries, Ltd., >99%), organic solvent (*n*-decane) was not used.

The used catalyst was washed with excess water, dried in air and then calcined at 773 K for 3 h. A slight loss (<15% in weight) was observed during the recovery process and was compensated with fresh catalyst in each reuse experiment. Before the activity test, the reduction pretreatment are carried out again in the same way as for the fresh catalyst. The amount of eluted metal during the reaction was analyzed by inductively coupled plasma atomic emission spectrometry (ICP-AES, Thermo Scientific iCAP 6500).

2.3. Catalyst characterization

Temperature-programmed reduction (TPR) was carried out in a fixed-bed reactor equipped with a thermal conductivity detector using 5% H_2 diluted with Ar (30 ml/min). The amount of catalyst was 0.05 g, and the temperature was increased from room temperature to 1123 K at a heating rate of 10 K/min.

X-ray diffraction (XRD) patterns were recorded by a diffractometer (Rigaku MiniFlex 600). Average metal particle size was estimated by using the Scherrer equation [49].

The X-ray absorption near-edge structure (XANES) spectra were measured at the BL01B1 station at SPring-8 with the approval of the Japan Synchrotron Radiation Research Institute (JASRI; Proposal No. 2015A1134). The storage ring was operated at 8 GeV, and a Si (1 1 1) single crystal was used to obtain a monochromatic X-ray beam. Two ion chambers for I_0 and I were filled with 85% N_2 + 15% Ar and 50% N_2 + 50% Ar, respectively, for Pt L_3-edge, Re L_3-edge and Ir L_3-edge measurements. We prepared the sample after the catalytic use as follows. The catalytic reaction was carried out in an autoclave. The reaction conditions were the same as in activity tests. After cooling, the wet catalyst powder was transferred to the measurement cell in

a glove bag filled with nitrogen. The thickness of the cell filled with the powder was 2 mm to give an edge jump of 0.7, 0.9 and 0.4 for Ir L_3-edge, Re L_3-edge and Pt L_3-edge measurement, respectively, in the case of Pt(3)-Ir-ReO_x/SiO_2. The EXAFS data were collected in a transmission mode. For EXAFS analysis, the oscillation was first extracted from the EXAFS data using a spline smoothing method [50]. Fourier transformation of the k^3-weighted EXAFS oscillation from the k space to the r space was performed to obtain a radial distribution function. The inversely Fourier filtered data were analyzed using a usual curve fitting method [51,52]. For curve fitting analysis, the empirical phase shift and amplitude function for the Re-O bond was extracted from data for NH_4ReO_4. Theoretical functions for the Re-Ir were calculated using the FEFF8.2 program [53]. The Re-Ir bond was represented by the Re-Ir (or -Re or -Pt), in the curve fitting results. This is because it is very difficult to distinguish among Pt, Ir and Re as a backscattering atom. Analyses of EXAFS data were performed using a computer program (REX2000, ver. 2.5.9; Rigaku Corp.). Error bars for each parameter were estimated by stepping each parameter, while optimizing the other parameters, until the residual factor becomes two times as its minimum value [54].

The amount of CO chemisorption was measured in a high-vacuum system using a volumetric method in the vacuum line. Before adsorption measurements, the catalysts were reduced in H_2 at 473 K for 1 h. The adsorption was conducted at room temperature. The equilibrium pressure, the sample weight and the dead volume of the apparatus were about 1.1 kPa, 0.15 g and 43 cm^3, respectively.

3. Results and discussion

3.1. Screening of catalysts for the conversion of sorbitol

The performances of various catalysts in the conversion of sorbitol are compared in Table 1. In our previous research, Ir-ReO_x/SiO_2 (Re/Ir = 2) showed good catalytic performance in conversion of sorbitol or cellulose to *n*-hexane or hexanols with high pressure H_2 in water + *n*-alkane biphasic solvent system where *n*-alkane acted as an extraction solvent for capturing the formed products [38,39,48]. However, when Ir-ReO_x/SiO_2 catalyst was used in Ar atmosphere, almost no gasoline-ranged products were formed (Entry 1). This could be attributed to the low performance in APR of sorbitol judging from the low yield of CO_2. The main detected product was isosorbide with the yield of 8.2% which was not shown in table. To improve the C—C cracking performance of Ir-ReO_x/SiO_2, another noble metal such as Ru, Pd, Rh and Pt was added (Entries 2–5). When Ru was added to Ir-ReO_x/SiO_2 catalyst, almost no APR activity was shown and the catalytic performance was almost the same as that of Ir-ReO_x/SiO_2 catalyst (Entry 2). Additions of Pd, Rh and Pt gave the catalyst APR activity (Entries 3–5). Significant amount of gasoline-ranged products were obtained, showing that the in situ produced H_2 was used for the successive hydrogenolysis reaction. In the cases of Pd and Rh modified Ir-ReO_x/SiO_2 catalysts, APR performance was improved moderately from Ir-ReO_x/SiO_2 while Pt modified Ir-ReO_x/SiO_2 catalyst showed the best APR performance. The order of gasoline-ranged products yields over these catalysts was as follows: Pt(5)-Ir-ReO_x/SiO_2 > Rh(5)-Ir-ReO_x/SiO_2 > Pd(5)-Ir-ReO_x/SiO_2. Of the mono-functionalized hydrocarbons formed over Pt-Ir-ReO_x/SiO_2, ketones were the predominant products. It should be noted that these ketones could be used as the precursors for the production of jet fuel by C—C coupling reaction and hydrodeoxygenation [55]. The amount of C5–C6 alkanes was much smaller than that of mono-functionalized hydrocarbons and these alkanes were mainly *n*-alkanes. No CO was detected. Therefore, Pt added Ir-ReO_x/SiO_2 catalyst was chosen for conversion of sorbitol without external hydrogen. The reactions of C—C and C—O dissociation were

Table 1
Conversion of sorbitol over different catalysts under Ar.

Entry	Catalyst	Conv., %	Yield, %													H_2, mmol
			Gasoline-ranged products										CO_2	Loss of carbon balance		
			Hexanones	HxOHs	Pentanones	PeOHs	Butanone	Acetone	Ethers	Acid	Hexanes	Pentanes	Sum	C4–C1 alkanes		
1	Ir-ReO_x/SiO_2	67.6	0.0	0.0	0.0	0.0	0.0	0.0	0.3	0.0	0.4	0.0	0.6	0.0	2.0	65	0.1
2	Ru(5)-Ir-ReO_x/SiO_2	69.8	0.1	0.2	0.1	0.0	0.0	0.0	0.1	0.5	0.1	0.3	1.4	0.3	4.1	64	0.0
3	Pd(5)-Ir-ReO_x/SiO_2	>99.9	1.5	0.5	0.1	0.0	0.5	0.0	7.8	1.4	0.5	0.4	13	0.6	22	64	1.8
4	Rh(5)-Ir-ReO_x/SiO_2	>99.9	2.2	1.1	3.0	0.3	2.1	0.1	0.9	2.1	2.1	2.7	16	3.1	29	52	1.8
5	Pt(5)-Ir-ReO_x/SiO_2	>99.9	11	3.4	3.5	1.0	0.5	0.3	4.8	6.0	4.8	3.8	39	3.2	41	16	2.0
6	Pt(3)-Ir-ReO_x/SiO_2	>99.9	11	4.4	3.5	1.5	1.2	0.3	5.4	5.9	5.1	3.8	42	3.2	35	19	2.0
7	Pt(2)-Ir-ReO_x/SiO_2	>99.9	7.1	1.5	2.8	0.5	1.0	0.1	4.0	3.5	2.9	2.2	26	2.8	27	46	1.1
8	Pt(1)-Ir-ReO_x/SiO_2	>99.9	3.2	1.1	2.2	0.9	1.1	0.4	2.0	6.2	1.2	1.0	19	1.1	20	60	0.3
9	Pt(0.5)-Ir-ReO_x/SiO_2	80.5	1.3	1.1	0.9	0.9	0.7	0.4	0.7	6.5	1.0	0.4	14	0.4	7.7	58	0.0
10	Pt(3)/SiO_2	10.5	0.0	0.0	0.0	0.0	0.0	0.0	0.0	0.0	0.0	0.0	0.0	0.0	0.5	10	0.1
12	Pt(3)-ReO_x/SiO_2	19.9	0.0	0.0	0.0	0.0	0.0	0.0	0.3	0.0	0.0	0.0	0.0	0.0	1.7	18	0.9
12	Pt(3)/SiO_2 + Ir-ReO_x/SiO_2	78.6	0.6	0.0	0.0	0.0	0.0	0.0	0.4	0.5	0.1	0.2	1.8	0.3	4.3	72	0.1
13	Pt(3)-Ir-ReO_x/SiO_2 [a]	>99.9	12	3.6	3.8	1.0	1.3	0.4	4.5	5.3	6.3	3.9	42	4.5	38	15	1.4
14	Pt(3)-Ir-ReO_x/SiO_2 [b]	>99.9	6.5	0.2	3.3	0.3	0.8	0.1	1.8	4.6	4.5	5.8	28	1.7	29	42	0.6

Hexanones: 2-hexanone and 3-hexanone; HxOH: 1-hexanol, 2-hexanol and 3-hexanol; pentanones: 2-pentanones and 3-pentanones; PeOH: 1-pentanol, 2-pentanol and 3-pentanol; ethers: 2-methyltetrahydrofuran, 2,5-dimethyltetrahydrofuran and 2-methyltetrahydropyran; hexanes: *n*-hexane, 2-methylpentane and 3-methylpentane; acid: acetic acid, propanoic acid, butanoic acid, valeric acid and hexanoic acid; C4–C1 alkanes: *n*-butane, propane, ethane and methane.
Reaction conditions: catalyst: 0.15 g, sorbitol: 0.5 g, H_2O: 9.5 g, initial Ar: 0.5 MPa, 453 K, 24 h (a: 48 h), *n*-decane: 20 ml (b: 0 ml).

involved in the production of gasoline-ranged products from sorbitol. Therefore, all the noble-metals modified Ir-ReO_x/SiO_2 should have bi-functional roles of the activities of APR and hydrogenolysis. On the one hand, Dumesic et al. have found that the overall catalytic performance for ethylene glycol reforming decreased in the following order for silica-supported metals: Pt > Ru > Rh ~ Pd > Ir [56]. Silica-supported Pt and Pd catalysts exhibited relatively high selectivities for production of H_2, while silica-supported Rh and Ru catalysts showed a low selectivity for production of H_2. This trend could be related to our results that the noble metals modified Ir-ReO_x/SiO_2 catalysts except Ru-modified Ir-ReO_x/SiO_2 showed. On the other hand, in our previous work, the activity of silica-supported metals in hydrogenolysis of glycerol decrease in the order: Ru > Rh > Pt, Pd while ReO_x modified silica-supported metals with the order: Rh-ReO_x > Ru-ReO_x > Pt-ReO_x > Pd-ReO_x. In addition, Ru, Rh and Pd modified Ir-ReO_x/SiO_2 showed that Ru improved the hydrogenolysis activity of Ir-ReO_x/SiO_2 while Rh and Pd showed negative effect, especially Pd [57,58]. The addition of Pt also improved the hydorgenolysis performance of Ir-ReO_x/SiO_2 which was shown below. This could be related to the yields of gasoline-ranged products over Pt, Rh and Pd modified catalyst.

To obtain high yield of gasoline-ranged products, controlling the relative rates of C—O and C—C cleavage is a key. Activity in C—C cleavage is important to obtain enough H_2 via APR, whereas much higher rate of C—C cleavage than C—O cleavage decreases the yield of products with larger carbon number, which are suitable for gasoline. Therefore, the effect of Pt loading amount of Pt-Ir-ReO_x/SiO_2 on the performance was investigated (Table 1, entries 5–9). The activity of APR, in terms of CO_2 yield, increased as the Pt loading amount increased. The sum yield of all the gasoline-ranged products increased when the loading amount increased to 3 wt%. When Pt loading amount was further increased to 5 wt%, the sum yield of the gasoline-ranged products decreased slightly. Therefore, Pt(3)-Ir-ReO_x/SiO_2 was chosen as the standard catalyst and the molar ratio of Pt:Ir:Re was 1:1.3:2.6 on this catalyst. Another important point is that Pt(3)/SiO_2, Pt(3)-ReO_x/SiO_2 and Ir-ReO_x/SiO_2 showed very low APR performance. Although the Re addition to Pt/SiO_2 enhanced the APR activity, the additive effect was not so significant. This can be because the reaction temperature (453 K) was significantly lower than that in the literature for APR over Pt- and Pt-Re catalysts (~500 K) and the different support materials [10,21–24]. The yield of gasoline-ranged products over the physical mixture of Pt(3)/SiO_2 and Ir-ReO_x/SiO_2 catalysts was much lower than those over Pt(3)-Ir-ReO_x/SiO_2 catalyst. This indicated the strong synergetic effect of Pt and Ir-ReO_x. The product yields and distributions were almost unchanged when the reaction time was prolonged (Entry 12). The conversion of sorbitol under pressurized H_2 was also conducted (Table S2). The main products were hexanols which was very different from that under Ar. The yield of hexanols over Pt(3)-Ir-ReO_x/SiO_2 was higher than that over Ir-ReO_x/SiO_2, which indicated that the addition of Pt improved the hydrogenolysis activity of Ir-ReO_x/SiO_2 in pressurized hydrogen.

When the reaction was conducted without sorbitol, almost no *n*-decane was converted. As a result, it is verified that the organic solvent was inert under the reaction condition. When the reaction was conducted without *n*-decane, the yield of gasoline-ranged products was much lower than that with *n*-decane. This can be attributed to the fact that the organic solvent (*n*-decane) not only capture the products with low-boiling point for analysis, but also suppress the consecutive reaction of intermediates with high solubility to alkanes. The product distribution in different phases is shown in Table S1. In fact, most of ketones were present in the organic phase. Lowering the reactive ketones or aldehydes in the aqueous phase containing catalysts can suppress the polymerization, which starts with bi-molecular reaction, to undesirable by-products (loss of carbon balance).

3.2. Effect of reaction temperature

Table 2 shows the effect of reaction temperature on conversion of sorbitol over Pt(3)-Ir-ReO_x/SiO_2 catalyst. The sum yield of CO_2 and gasoline-ranged products increased as the reaction temperature was increased from 443 to 463 K. The amount of remaining H_2 was not so changed by the temperature change. This behavior indicated that higher temperature improved the APR activity efficiently to give larger amount of in situ hydrogen which was used in the C—O hydrogenolysis reactions. The hydrogenolysis activity of Ir-ReO_x/SiO_2 catalyst also increases with the increase in the reaction temperature [41]. In addition, the addition of Pt improved the hydrogenolysis activity of Ir-ReO_x/SiO_2 in pressurized hydrogen (Table S2). The yield of CO_2 decreased slightly with further increase of the reaction temperature (Entry 4). That could be attributed to faster growth rate of C—O dissociation than that of C—C cleavage with the increasing temperature, and more amount of sorbitol was consumed by C—O dissociation. The highest yield of gasoline-ranged products reached 42% when the reaction temperature was at the range of 453–463 K (Entry 2 and 3). However the yield of C5–C6 alkanes at 463 K was higher than that at 453 K.

3.3. Effect of HZSM-5 addition

Although over 40% yield of gasoline-ranged products can be produced over Pt(3)-Ir-ReO_x/SiO_2 catalyst, of them, over 65% of the products are oxygen-containing organic compounds which may not meet the gasoline requirement. Therefore further hydrodeoxygenation of products to alkanes would be preferred. To obtain high yield of alkanes, increasing the rate of C—O hydrogenolysis of Pt(3)-Ir-ReO_x/SiO_2 catalyst may be the key. It was reported that the addition of solid acids such as HZSM-5 can enhance the C—O hydrogenolysis activity of Ir-ReO_x/SiO_2 catalyst [44]. The combination of Ir-ReO_x/SiO_2 catalyst and HZSM-5 showed excellent performance in production of alkanes from cellulose or sugar alcohols with external hydrogen [38,39]. When HZSM-5 was used as co-catalyst in conversion of sorbitol without hydrogen, the total yield of gasoline-ranged products decreased slightly (Table 3). However, the distribution of products changed significantly. The yield of C5–C6 alkanes much increased while the oxygen-containing organic compounds decreased (Entry 2), indicating that HZSM-5 also improved the C—O cleavage performance of Pt(3)-Ir-ReO_x/SiO_2 catalyst. The yield of H_2 was much lower than that without HZSM-5, indicating that almost all of the hydrogen was consumed by hydrogenolysis reaction. At longer reaction time, the yield of C5–C6 alkanes was slightly increased (30%) and the amount of them accounts for about 75% of the total gasoline-ranged products (Entry 3). The yield of CO_2 was almost the same as that without HZSM-5 indicating that HZSM-5 did not affect the APR performance of Pt(3)-Ir-ReO_x/SiO_2 catalyst. Almost no mono-alcohols were detected with the addition of HZSM-5 and the yield of ketones decreased gradually with the reaction time. The results suggest that the mechanism of hydrogenolysis of mono-alcohols and ketones proceeded by dehydration + hydrogenation and hydrogenation + dehydration + hydrogenation, respectively (Scheme 1). In particular, it has been reported that Ir-ReO_x/SiO_2 showed high activity in the hydrogenation of C=O bond [47]. The production of C5–C6 alkanes especially hexanes was limited by the hydrogenation of ketones. The addition of HZSM-5 not only enhanced the dehydration of mono-alcohols, but also improved the ketones hydrogenation performance of Pt(3)-Ir-ReO_x/SiO_2 catalyst.

3.4. Catalyst stability

Table 4 lists the results of the reuse test of Pt(3)-Ir-ReO_x/SiO_2. The yield of gasoline-ranged products was decreased gradually

Table 2
Reaction temperature effect on conversion of sorbitol over Pt(3)-Ir-ReO_x/SiO_2 under Ar.

Entry	T, K	Conv., %	Yield, %														
			Gasoline-ranged products											C4–C1 alkanes	CO_2	Loss of carbon balance	H_2, mmol
			Hexanones	HxOHs	Pentanones	PeOHs	Butanone	Acetone	Ethers	Acid	Hexanes	Pentanes	Sum				
1	443	>99.9	8.3	2.2	2.5	1.1	0.7	0.2	4.2	4.8	3.4	2.4	30	1.4	26	43	1.1
2	453	>99.9	11	4.4	3.5	1.5	1.2	0.3	5.4	5.9	5.1	3.8	42	3.2	35	19	2.0
3	463	>99.9	12	1.5	4.0	0.4	1.1	0.3	2.7	4.4	9.1	6.7	42	3.8	42	13	1.4
4	473	>99.9	13	1.9	4.3	0.7	1.2	0.3	2.4	4.4	7.4	6.2	41	3.9	38	17	1.6

Hexanones: 2-hexanone and 3-hexanone; HxOH: 1-hexanol, 2-hexanol and 3-hexanol; pentanones: 2-pentanones and 3-pentanones; PeOH: 1-pentanol, 2-pentanol and 3-pentanol; ethers: 2-methytetrahydrofuran, 2,5-dimethyltetrahydrofuran and 2-methyltetrahydropyran; hexanes: *n*-hexane, 2-methylpentane and 3-methylpentane; acid: acetic acid, propanoic acid, butanoic acid, valeric acid and hexanoic acid; C4-C1 alkanes: *n*-butane, propane, ethane and methane.
Reaction conditions: catalyst: 0.15 g, sorbitol: 0.5 g, H_2O: 9.5 g, initial Ar: 0.5 MPa, 24 h, *n*-decane: 20 ml.

Table 3
The addition of HZSM-5 effect on conversion of sorbitol over Pt(3)-Ir-ReO_x/SiO_2.

Entry	HZSM-5, g	Conv., %	Yield, %														
			Gasoline-ranged products											C4–C1 alkanes	CO_2	Loss of carbon balance	H_2, mmol
			Hexanones	HxOHs	Pentanones	PeOHs	Butanone	Acetone	Ethers	Acid	Hexanes	Pentanes	Sum				
1	0.0	>99.9	12	1.5	4.0	0.4	1.1	0.3	2.7	4.4	9.1	6.7	42	3.8	42	13	1.4
2	0.06	>99.9	5.3	0.0	1.7	0.0	0.5	0.2	0.2	4.4	16	9.3	38	4.2	42	16	0.1
3[a]	0.06	>99.9	3.1	0.0	1.0	0.0	0.3	0.2	0.2	5.1	19	11	40	5.3	43	12	0.1

Hexanones: 2-hexanone and 3-hexanone; HxOH: 1-hexanol, 2-hexanol and 3-hexanol; pentanones: 2-pentanones and 3-pentanones; PeOH: 1-pentanol, 2-pentanol and 3-pentanol; ethers: 2-methytetrahydrofuran, 2,5-dimethyltetrahydrofuran and 2-methyltetrahydropyran; hexanes: *n*-hexane, 2-methylpentane and 3-methylpentane; acid: acetic acid, propanoic acid, butanoic acid, valeric acid and hexanoic acid; C4-C1 alkanes: *n*-butane, propane, ethane and methane.
Reaction conditions: catalyst: 0.15 g, sorbitol: 0.5 g, H_2O: 9.5 g, initial Ar: 0.5 MPa, 463 K, *n*-decane: 20 ml, 24 h (a: 48 h).

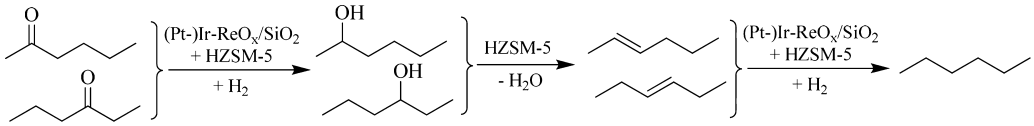

Scheme 1. Reaction routes for conversion of hexanones to *n*-hexane.

Table 4
Reusability of Pt(3)-Ir-ReO_x/SiO_2 for conversion of sorbitol under Ar.

Entry	Usage	Conv., %	Yield, %														
			Gasoline-ranged products											C4-C1 alkanes	CO_2	Loss of carbon balance	H_2, mmol
			Hexanones	HxOHs	Pentanones	PeOHs	Butanone	Acetone	Ethers	Acid	Hexanes	Pentanes	Sum				
1	1	>99.9	11	4.4	3.5	1.5	1.2	0.3	5.4	5.9	5.1	3.8	42	3.2	35	20	2.0
2	2	>99.9	6.9	0.7	2.7	1.1	0.6	0.2	4.0	5.0	3.3	2.8	27	1.7	32	39	1.3
3	3	>99.9	5.4	0.1	2.5	0.5	0.4	0.2	3.3	3.4	2.3	2.2	20	1.3	29	49	0.9

Hexanones: 2-hexanone and 3-hexanone; HxOH: 1-hexanol, 2-hexanol and 3-hexanol; pentanones: 2-pentanones and 3-pentanones; PeOH: 1-pentanol, 2-pentanol and 3-pentanol; ethers: 2-methytetrahydrofuran, 2,5-dimethyltetrahydrofuran and 2-methyltetrahydropyran; hexanes: *n*-hexane, 2-methylpentane and 3-methylpentane; acid: acetic acid, propanoic acid, butanoic acid, valeric acid and hexanoic acid; C4-C1 alkanes: *n*-butane, propane, ethane and methane.
Reaction conditions: catalyst: 0.15 g, sorbitol: 0.5 g, H_2O: 9.5 g, initial Ar: 0.5 MPa, 453 K, 24 h, *n*-decane: 20 ml.

with reuses while the yield of CO_2 was decreased slightly. This indicated that Pt(3)-Ir-ReO_x/SiO_2 was deactivated in C—O hydrogenolysis while the APR performance of the catalyst was almost maintained. To identify the cause of the catalyst deactivation, ICP and XRD characterizations were conducted. Inductively coupled plasma (ICP) analysis of the reaction solution after the filtration of catalyst showed almost no leaching of Ir and Pt (<0.05%) and slight leaching of Re (1.0–2.7% for each run). The XRD peaks (Fig. S1) of the catalysts after the 3rd run became sharper than those of the catalysts after reduction and the 1st reaction, indicating the aggregation of metal during reaction and regeneration. The aggregation could be the reason for the decrease in the gasoline-ranged products formation. Similar decrease in activity by aggregation was observed for Ir-ReO_x/SiO_2 [39,48], Pd-Ir-ReO_x/SiO_2 [59] and Rh-Ir-ReO_x/SiO_2 [58] in the conversion of cellulose or furfural with hydrogen.

3.5. Characterization of catalyst

The profiles of temperature-programmed reduction (TPR) of Pt(3)/SiO_2, Ir/SiO_2, ReO_x/SiO_2, Pt(3)-Ir/SiO_2, Pt(3)-ReO_x/SiO_2, Ir-ReO_x/SiO_2 and Pt(3)-Ir-ReO_x/SiO_2 after calcination are shown in Fig. 1. The H_2 consumption amount and the summary of other characterizations are shown in Table 5. Pt(3)/SiO_2 was reduced at low temperature (Fig. 1a). Ir/SiO_2 was completely reduced at 600 K (Fig. 1b) while ReO_x/SiO_2 was partially reduced at 800 K to the

Table 5
Summary of characterization results.

Catalyst	Metal amount, mmol g_{cat}^{-1}			TPR		Re L_3-edge XANES	Particle size, nm		CO adsorption, mmol g_{cat}^{-1}	Dispersion[b], %
	Pt	Ir	Re	H_2 consumption, mmol g_{cat}^{-1}	Valence of Re[a]	Valence of Re	XRD	TEM		
Pt(3)/SiO_2	0.15	–	–	0.08	–	–	25.9	23.4	0.002	1.3
Ir/SiO_2	–	0.21	–	0.40	–	–	3.6	–	–	–
ReO_x/SiO_2	–	–	0.42	1.13	1.6	–	–	–	–	–
Pt(3)-ReO_x/SiO_2	0.15	–	0.40	0.37	5.2	–	14.9	–	–	–
Pt(3)-Ir/SiO_2	0.15	0.20	–	0.39	–	–	6.3	–	–	–
Ir-ReO_x/SiO_2	–	0.21	0.42	0.93	4.5	3.1	2.1	–	0.037	18
Pt(3)-Ir-ReO_x/SiO_2	0.15	0.20	0.40	1.06	3.7	2.5	3.1	3.8	0.083	23

[a] $7 - 2 \times$ [(amount of H_2 consumed, mol) $- 2 \times$ (Ir loading amount, mol)]/(Re loading amount, mol).
[b] Dispersion (%) = [CO adsorption amount]/[(Ir loading amount) + (Pt loading amount)] $\times$ 100.

Table 6
Re L_3-edge EXAFS curve fitting results of the catalysts.

Catalyst	Shells	CN[a]	R, 10^{-1} nm[b]	σ, 10^{-1} nm[c]	ΔE_0, eV[d]	R_f, %[e]
Ir-ReO_x/SiO_2[f]	Re-O	1.7 ± 0.5	2.03 ± 0.02	0.080 ± 0.016	0.6 ± 5.0	2.5
	Re-Ir (or -Re)	6.1 ± 1.1	2.68 ± 0.01	0.082 ± 0.006	8.1 ± 1.8	
Pt(3)-Ir-ReO_x/SiO_2[g]	Re-O	1.2 ± 0.5	2.08 ± 0.02	0.088 ± 0.010	8.1 ± 1.0	1.8
	Re-Ir (or -Re or -Pt)	8.0 ± 1.0	2.68 ± 0.01	0.077 ± 0.005	7.9 ± 1.5	
NH_4ReO_4	Re=O	4	1.73	0.060	0	–

[a] Coordination number.
[b] Bond distance.
[c] Debye-Waller factor.
[d] Difference in the origin of photoelectron energy between the reference and the sample.
[e] Residual factor.
[f] After hydrogenolysis of glycerol, Ref. [39].
[g] After reduction. Fourier filtering range: 0.150–0.328 nm.

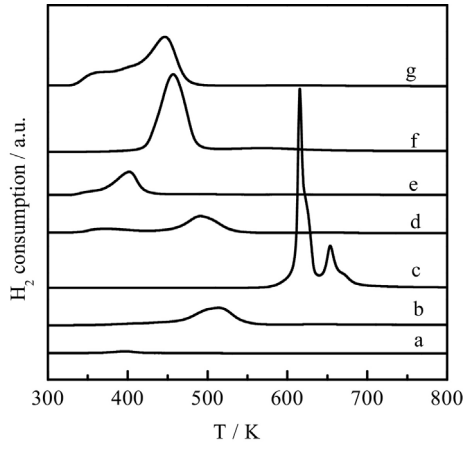

Fig. 1. TPR profiles of various catalysts after calcination: (a) Pt(3)/SiO_2, (b) Ir/SiO_2, (c) ReO_x/SiO_2, (d) Pt(3)-Ir/SiO_2, (e) Pt(3)-ReO_x/SiO_2, (f) Ir-ReO_x/SiO_2 and (g) Pt(3)-Ir-ReO_x/SiO_2. The H_2 consumption amount of each sample was shown in Table 6.

valence of +1.6 (Fig. 1c) from +7. In the cases of the bimetallic catalysts, Ir-ReO_x/SiO_2 showed only one large peak centered at around 460 K (Fig. 1f). Pt(3)-ReO_x/SiO_2 showed one peak centered at about 401 K (Fig. 1e). The area in the profile of Pt(3)-ReO_x/SiO_2 corresponded to the reduction of Re species to the valence of 5.2 while Pt was assumed to be reduced before heating. Pt(3)-Ir/SiO_2 showed two peaks at 373 K and 491 K. In the case of Pt(3)-Ir-ReO_x/SiO_2 catalyst, a broad signal appeared and the reduction ended at 490 K. The peak areas in the profiles of Ir-ReO_x/SiO_2 and Pt(3)-Ir-ReO_x/SiO_2 corresponded to the reduction of Re species to the valences of 4.5 and 3.7, respectively, in addition to the total reduction of Ir from Ir^{4+} while Pt was assumed to be reduced before heating (Table 6).

Fig. 2 shows the XRD patterns of Pt(3)/SiO_2, Ir/SiO_2, ReO_x/SiO_2, Pt(3)-Ir/SiO_2, Pt(3)-ReO_x/SiO_2, Ir-ReO_x/SiO_2, and Pt(3)-Ir-ReO_x/SiO_2 after reduction with 8 MPa H_2 at 473 K for 1 h. In the cases of monometallic catalysts, Pt(3)/SiO_2 displayed the peaks at $2\theta = 39.7°$, 46.2° and 67.4° which were assigned to Pt metal [60]. Ir/SiO_2 showed the peaks at $2\theta = 41.3°$, 47.3° and 69.1° which were assigned to Ir metal [61]. ReO_x/SiO_2 showed small peaks at $2\theta = 37.5°$, 40.5° and 42.9° which were assigned to Re metal [62]. It should be noted that most Re species were in the oxidized state based on the TPR results and XANES results shown below. In the cases of bimetallic catalysts, Pt(3)-ReO_x/SiO_2 showed the pattern which was similar to Pt(3)/SiO_2 but the peak of metal (1 1 1) was shifted to higher angle indicating the formation of Pt-Re alloy. Pt(3)-Ir/SiO_2 exhibited three tailing peaks and the main peak was shift to higher angle reflecting the formation of Pt-Ir alloy. Ir-ReO_x/SiO_2 showed the pattern whose peak positions were almost the same as those of Ir/SiO_2 while the peaks were broadened by the addition of Re, as reported earlier [41]. In the case of Pt-added Ir-ReO_x/SiO_2 catalysts, the XRD patterns of Pt(3)-Ir-ReO_x/SiO_2 became broader compared to Pt(3)-Ir/SiO_2 and the peak of metal (1 1 1) plane (around 40.2°) was between Pt metal and Ir metal, suggesting the formation of Pt-Ir alloy phase. However, the overlap of two different monometallic phases cannot be ruled out. According to the previous reports, the alloying of Ir with Pd and Rh was verified by XRD, TEM, EXAFS and so on [58,63]. According to Scherrer equation [49], the average particle size of Pt metal particle at Pt(3)/SiO_2 was 25.9 nm while the average metal particle size of Pt-Ir alloy was about 3.1 nm, although this value might be underestimated because of the heterogeneity of alloy compositions. Fig. 3 shows the TEM images of reduced Pt(3)/SiO_2 and Pt(3)-Ir-ReO_x/SiO_2. Metal nanoparticles were observed with narrow distribution of size. The average size of Pt(3)/SiO_2 was 23.4 nm while the average size of Pt(3)-Ir-ReO_x/SiO_2 was 3.8 nm. The values were similar to those calculated by XRD. The higher dispersion

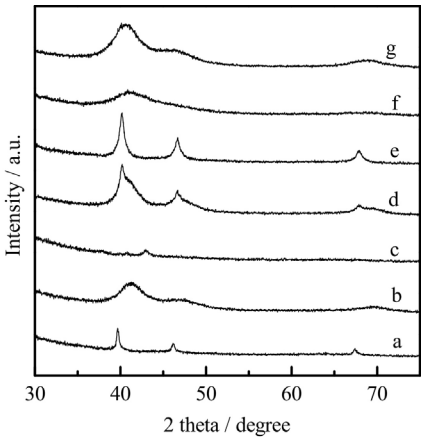

Fig. 2. XRD patterns of various catalysts: (a) Pt(3)/SiO_2, (b) Ir/SiO_2, (c) ReO_x/SiO_2, (d) Pt(3)-Ir/SiO_2, (e) Pt(3)-ReO_x/SiO_2, (f) Ir-ReO_x/SiO_2 and (g) Pt(3)-Ir-ReO_x/SiO_2.

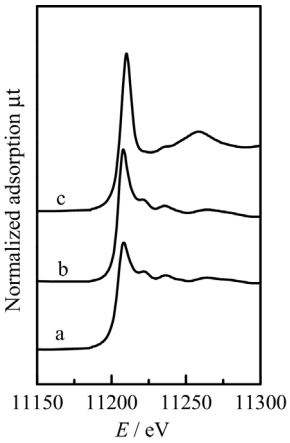

Fig. 4. Ir L_3-edge XANES spectra of Pt(3)-Ir-ReO_x/SiO_2. (a) Ir powder, (b) Pt(3)-Ir-ReO_x/SiO_2 after reduction, (c) IrO_2.

at Pt(3)-Ir-ReO_x/SiO_2 catalyst was also proved by the CO adsorption of Pt(3)/SiO_2, Ir-ReO_x/SiO_2 and Pt(3)-Ir-ReO_x/SiO_2 catalysts. The adsorption amount of CO on Pt(3)/SiO_2 was 0.002 mmol g_{cat}^{-1} (CO/Pt = 1.3%) while the adsorption amount of CO on Pt(3)-Ir-ReO_x/SiO_2 catalyst was 0.083 mmol g_{cat}^{-1} (CO/(Pt + Ir) = 23%). The amount of CO adsorption on Ir-ReO_x/SiO_2 was 0.037 mmol g_{cat}^{-1} (CO/Ir = 18%). The CO/(Pt + Ir) value was higher than the CO/Ir of Ir-ReO_x/SiO_2, while the size of metal particles of Pt(3)-Ir-ReO_x/SiO_2 (~4 nm) was larger than that of Ir-ReO_x/SiO_2 (~2 nm) where Ir metal particles were partially covered with ReO_x species [41]. The large CO/(Pt + Ir) value suggests that the Pt-Ir alloy particles were less covered by ReO_x species. Therefore, surface Pt sites are suggested to be less likely covered with ReO_x species than surface Ir site. The large number of surface Pt site would be connected to high performance in the APR of sorbitol.

Figs. 4–6 show the Ir L_3-, Pt L_3-, and Re L_3-XANES spectra of Pt(3)-Ir-ReO_x/SiO_2 and reference compounds, and the relation between white line area and valence of Re. In the cases of Ir and Pt species (Figs. 4 and 5), the white line features as well as the near-edge spectra were similar to the spectra of the Ir powder and Pt foil, respectively, which reflected that Ir and Pt species were in reduced state after reduction at 473 K. In the case of Re species, Re was not reduced completely (Fig. 6), which agreed with the TPR results. The valence of Re species was estimated by examining the white line area in the XANES spectra [64–66]. The valence of Re species in Ir-ReO_x/SiO_2 was 3.1 while the valence of Re species in Pt(3)-Ir-ReO_x/SiO_2 was 2.5. In concord with TPR results, the valence of Re in Pt(3)/Ir-ReO_x/SiO_2 was similar to that of Ir–ReO_x/SiO_2. The difference in the valence from the XANES analysis and TPR can be explained by the difference of pretreatment conditions between P_{H2} = 8 MPa in water in XANES/EXAFS measurement and

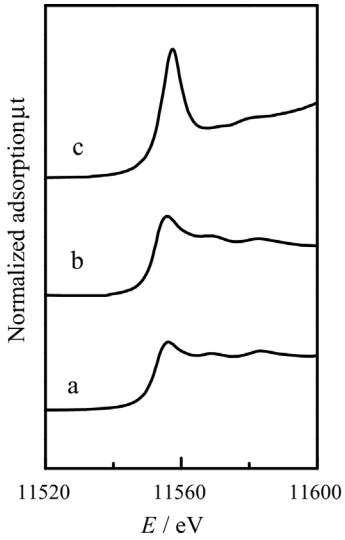

Fig. 5. Pt L_3-edge XANES spectra of Pt(3)-Ir-ReO_x/SiO_2. (a) Pt foil, (b) Pt(3)-Ir-ReO_x/SiO_2 after reduction, (c) PtO_2.

P_{H2} = 5.05 kPa in N_2 flow in TPR. Similar tendency in the valence difference was also observed in the cases of Ir-ReO_x/SiO_2 [41,45] and Pt-ReO_x/SiO_2 [64,65], Rh-ReO_x/SiO_2 [67].

Further characterization of Pt(3)-Ir-ReO_x/SiO_2 catalyst was carried out using Ir L_3-edge, Re L_3-edge and Pt L_3-edge EXAFS and the detailed spectra and analyses are shown in Fig. S2. As is known, the edge energy of Pt and Ir was close, and thereby the spectra of Pt L_3-edge and Ir L_3-edge were overlapped. Therefore, curve fitting was

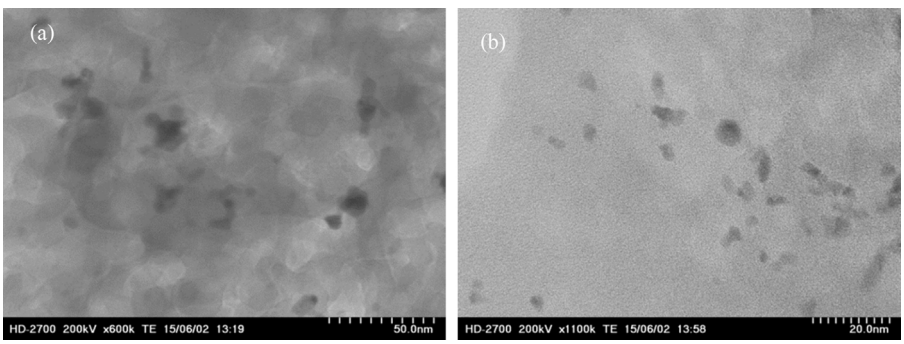

Fig. 3. TEM images of various catalysts: (a) Pt(3)/SiO_2 and (b) Pt(3)-Ir-ReO_x/SiO_2.

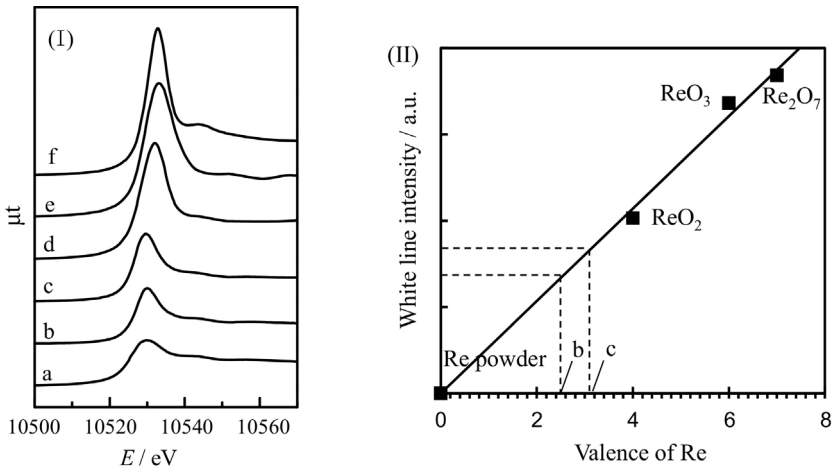

Fig. 6. Results of Re L_3-edge XANES analysis of Ir-ReO_x/SiO_2 and Pt(3)-Ir-ReO_x/SiO_2. (I) Re L_3-edge XANES spectra, (II) Relation between white line area and valence of Re. (a) Re powder, (b) Pt(3)-Ir-ReO_x/SiO_2 after reduction, (c) Ir-ReO_x/SiO_2 after the catalytic use, and (d) ReO_2, (e) ReO_3 and (f) Re_2O_7.

Table 7
Conversion of glycerol over different catalysts.

Entry	Catalyst	Conv., %	Selectivity, %													
			1,2-PrD	1-PrOH	2-PrOH	Acetol	EG	EtOH	Methanol	Propanoic acid	Acetic acid	C_3H_8	C_2H_6	CH_4	CO_2	CO	H_2
1	Pt(3)-Ir-ReO_x/SiO_2	34.0	12.2	18.6	1.1	5.7	2.7	8.4	0.0	3.0	1.9	4.5	2.3	0.8	23.0	0.0	7.0
2	Pt(3)/SiO_2 + Ir-ReO_x/SiO_2	7.3	9.6	0.0	0.0	69.4	2.2	0.0	0.0	1.0	0.8	2.5	1.1	0.3	10.7	0.2	13.2
3	Pt(3)/SiO_2	2.7	0.0	0.0	0.0	65.7	0.0	14.9	0.0	0.0	0.0	0.3	0.5	0.2	18.1	0.3	29.0
4	Ir/SiO_2	0.8	0.0	0.0	0.0	88.6	0.0	0.0	0.0	0.0	0.0	1.0	0.0	0.0	5.2	1.5	52.9
5	ReO_x/SiO_2	0.0	0.0	0.0	0.0	0.0	0.0	0.0	0.0	0.0	0.0	0.0	0.0	0.0	0.0	0.0	0.0
6	Ir-ReO_x/SiO_2	5.5	8.7	0.0	0.0	77.1	0.6	0.0	0.0	1.5	0.0	3.2	1.0	0.3	5.0	0.2	11.5
7	Pt(3)-ReO_x/SiO_2	3.4	0.0	0.0	0.0	70.1	0.0	2.3	0.0	0.0	0.0	3.4	1.5	0.5	21.7	0.4	21.3
8	Pt(3)-Ir/SiO_2	7.1	10.8	0.0	4.7	41.0	5.9	5.5	0.0	0.0	0.0	0.6	0.6	0.3	27.3	0.2	28.1

1,2-PrD: 1,2-propanediol, EG: ethylene glycol, PrOH: propanol, EtOH: ethanol.
Reaction Conditions: catalyst 0.1 g, glycerol 2 g, H_2O 18 g, 463 K, Ar 2 MPa, 4 h.
Selectivity to hydrogen was calculated with the formula: (mol of H_2)/(moles of glycerol converted)/7 × 100.

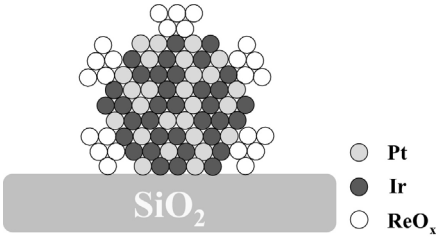

Fig. 7. A model structure of Pt(3)-Ir-ReO_x/SiO_2 catalyst.

carried out only for Re L_3-edge EXAFS spectra (Table 7). The spectra can be fitted by Re-O shell and Re-Ir (-Re or Pt). The existence of Re-O shell shows that Re was not reduced completely after reduction. The coordination number (CN) of Re-Ir (or -Re or Pt) of Pt(3)-Ir-ReO_x/SiO_2 was slightly higher than that of Ir-ReO_x/SiO_2. According to the previous report, the structure of Ir-ReO_x/SiO_2 catalyst was supported Ir metal partially covered with three-dimensional ReO_x clusters [41]. The valence of Re on Pt(3)-Ir-ReO_x/SiO_2 was lower than that on Ir-ReO_x/SiO_2, and this can increase the size of ReO_x clusters and the CN of Re-metal bond. The incorporation of small amount of Re metal into Pt-Ir alloy particles is difficult to be excluded.

Therefore, based on the above results on the structural analysis, Pt(3)-Ir-ReO_x/SiO_2 catalyst has the structure where Pt-Ir alloy particles were formed and ReO_x species are located on the alloy particles (Fig. 7).

3.6. Role of catalyst component

To understand the functions of different components of Pt(3)-Ir-ReO_x/SiO_2 catalyst, different catalysts were tested for conversion of glycerol as a model substrate without external hydrogen (Table 7). In the cases of Ir/SiO_2 and ReO_x/SiO_2 catalysts, almost no glycerol was converted (Entries 4 and 5). Ir-ReO_x/SiO_2 showed almost no APR activity and the main product was acetol which is the dehydration product of glycerol (Entry 6). This agreed with the result of sorbitol conversion that isosorbide was the main detected product over Ir-ReO_x/SiO_2. In the case of Pt/SiO_2 catalyst, the activity was very low which could be related to the large particle size of Pt metal (Entry 3). The main reaction pathways are dehydration and APR. When Pt was added to ReO_x/SiO_2 and Ir/SiO_2 catalysts, the conversion of glycerol and APR activity was slightly improved (Entries 7 and 8). Pt-Ir/SiO_2 showed better performance, which could be related to the smaller size of Pt-Ir alloy as shown by XRD. The mixture of Pt/SiO_2 and Ir-ReO_x/SiO_2 showed almost the same conversion of glycerol as Pt-Ir/SiO_2 while the selectivity to CO_2 was lower compared to that of Pt-Ir/SiO_2 catalyst (Entries 2 and 8). This shows that Pt-Ir alloy plays an important role in the APR reaction. When Pt was added to Ir-ReO_x/SiO_2, the conversion of glycerol increased significantly compared to the mixture of Pt/SiO_2 and Ir-ReO_x/SiO_2, indicating their strong synergetic effect (Entries 1 and 2). Although the CO_2 selectivity was a little lower than that over Pt-Ir/SiO_2 catalyst, the selectivity to hydrogenolysis products such as 1,2-propanediol, 1-propanol and alkanes were much higher. This suggested that Pt-Ir alloy modified with ReO_x exhibited high C—O hydrogenolysis performance by using in situ generated hydrogen.

In addition, no CO was detected over Pt(3)-Ir-ReO_x/SiO_2 catalyst indicating that the catalyst also has high activity in the water-gas shift reaction. Hensen et al. reported that the overall APR catalytic performance strongly correlates with the activity trend for the water-gas shift reaction and Pt and Re showed strong synergetic effect on the APR of glycerol [68]. This could also explained the results that Pt(3)-Ir-ReO_x/SiO_2 showed the best performance on APR of glycerol.

4. Conclusions

Pt-modified Ir-ReO_x/SiO_2 catalyst was effective in the production of gasoline-ranged products including C5–C6 alkanes and C2–C6 mono-functionalized compounds such as ketones, alcohols, cyclic ethers and carboxylic acids from sorbitol without external hydrogen. Addition of Ru, Pd and Rh showed small effect. The highest yield of gasoline-ranged products reached 42% over the Pt(3 wt%)-Ir-ReO_x/SiO_2 catalyst. The addition of HZSM-5 results in significant changes in the products' distribution. When Pt(3)-Ir-ReO_x/SiO_2 combined with HZSM-5, the main products were C5–C6 alkanes. On the other hand, the main products were C2–C6 mono-functionalized compounds without addition of HZSM-5. Characterizations by TPR, XRD, TEM, XANES, EXAFS, CO adsorption suggested that Pt(3)-Ir-ReO_x/SiO_2 catalyst has the structure of Pt-Ir alloy particles partially covered with ReO_x species, and surface Pt sites are less covered. The large number of Pt surface sites gives good performance of aqueous phase reforming performance which produces hydrogen for hydrogenolysis reaction catalyzed by Ir-ReO_x. The synergetic effect of Pt, Ir, ReO_x species plays an important role in the formation of gasoline-ranged products through C—O cleavage by utilizing in situ generated hydrogen under Ar atmosphere.

Acknowledgements

This work was in part supported by the JSPS KAKENHI 26249121. Sibao Liu thanks the China Scholarship Council (CSC) for the financial support. We also acknowledge the Technical Division in the School of Engineering in Tohoku University for TEM measurements.

Appendix A. Supplementary data

Supplementary material related to this article can be found, in the online version, at http://dx.doi.org/10.1016/j.cattod.2015.10.023.

References

[1] G.W. Huber, S. Iborra, A. Corma, Chem. Rev. 106 (2006) 4044–4098.
[2] J.C. Serrano-Ruiz, R. Luque, A. Sepulveda-Escribano, Chem. Soc. Rev. 40 (2011) 5266–5281.
[3] A. Corma, S. Iborra, A. Velty, Chem. Rev. 107 (2007) 2411–2502.
[4] M. Schlaf, Dalton Trans. (2006) 4645–4653.
[5] C.-H. Zhou, X. Xia, C.-X. Lin, D.-S. Tong, J. Beltramini, Chem. Soc. Rev. 40 (2011) 5588–5617.
[6] Y. Nakagawa, M. Tamura, K. Tomishige, J. Mater. Chem. A 2 (2014) 6688–6702.
[7] H. Kobayashi, A. Fukuoka, Green Chem. 15 (2013) 1740–1763.
[8] M. Besson, P. Gallezot, C. Pinel, Chem. Rev. 114 (2014) 1827–1870.
[9] Y. Nakagawa, S. Liu, M. Tamura, K. Tomishige, ChemSusChem 8 (2015) 1114–1132.
[10] G.W. Huber, R.D. Cortright, J.A. Dumesic, Angew. Chem. Int. Ed. 43 (2004) 1549–1551.
[11] N. Li, G.W. Huber, J. Catal. 270 (2010) 48–59.
[12] N. Li, G.A. Tompsett, G.W. Huber, ChemSusChem 3 (2010) 1154–1157.
[13] Y.T. Kim, J.A. Dumesic, G.W. Huber, J. Catal. 304 (2013) 72–85.
[14] B.M. Moreno, N. Li, J. Lee, G.W. Huber, M.T. Klein, RSC Adv. 3 (2013) 23769–23784.
[15] J. Duan, Y.T. Kim, H. Lou, G.W. Huber, Catal. Today 234 (2014) 66–74.
[16] L. Vilcoca, A. Cabiac, C. Especel, E. Guillon, D. Duprez, Catal. Commun. 15 (2011) 18–22.
[17] L. Vilcoca, A. Cabiac, C. Especel, E. Guillon, D. Duprez, Catal. Today 189 (2012) 117–122.
[18] L. Vilcoca, A. Cabiac, C. Especel, E. Guillon, D. Duprez, J. Catal. 320 (2014) 16–25.
[19] L. Vilcoca, A. Cabiac, C. Especel, E. Guillon, D. Duprez, Catal. Today 242 (2015) 91–100.
[20] L. Vilcoca, A. Cabiac, C. Especel, E. Guillon, D. Duprez, Appl. Catal. B: Environ. 148–149 (2014) 499–508.
[21] R.D. Cortright, R.R. Davda, J.A. Dumesic, Nature 418 (2002) 964–967.
[22] E.L. Kunkes, D.A. Simonetti, R.M. West, J.C. Serrano-Ruiz, C.A. Gärtner, J.A. Dumesic, Science 322 (2008) 417–421.
[23] A.V. Kirilin, A.V. Tokarev, E.V. Murzina, L.M. Kustov, J.-P. Mikkola, D.Y. Murzin, ChemSusChem 4 (2010) 708–718.
[24] A.V. Kirilin, A.V. Tokarev, L.M. Kustov, T. Salmi, J.-P. Mikkola, D.Y. Murzin, Appl. Catal. A: Gen. 172 (2012) 435–436.
[25] E. D'Hondt, S.V. Vyver, B.F. Sels, P.A. Jacobs, Chem. Commun. (2008) 6011–6012.
[26] A. Martin, U. Armbruster, I. Gandarias, P.L. Arias, Eur. J. Lipid Sci. Technol. 115 (2013) 9–27.
[27] A. Yin, X. Guo, W. Dai, K. Fan, Green Chem. 11 (2009) 1514–1516.
[28] B.B. Mane, C.V. Rode, Green Chem. 14 (2012) 2780–2789.
[29] J. Hu, Y. Fan, Y. Pei, M. Qiao, K. Fan, X. Zhang, B. Zong, ACS Catal. 3 (2013) 2280–2287.
[30] A. Iriondo, J.F. Cambra, V.L. Barrio, M.B. Guemez, P.L. Arias, M.C. Sanchez-Sanchez, R.M. Navarro, J.L.G. Fierro, Appl. Catal. B: Environ. 106 (2011) 83–93.
[31] C. Pendem, P. Gupta, N. Chaudhary, S. Singh, J. Kumar, T. Sasaki, A. Datta, R. Bal, Green Chem. 14 (2012) 3107–3113.
[32] M.L. Barbelli, G.F. Santori, N.N. Nichio, Bioresour. Technol. 111 (2012) 500–503.
[33] D. Roy, B. Subramaniam, R.V. Chaudhari, Catal. Today 156 (2010) 31–37.
[34] J. Zhang, F. Lu, W. Yu, J. Chen, S. Chen, J. Gao, J. Xu, Catal. Today 234 (2014) 107–112.
[35] S.V. Vyver, J. Geboers, P.A. Jacobs, B.F. Sels, ChemCatChem 3 (2011) 82–94.
[36] H. Kobayashi, T. Komanoya, S.K. Guha, K. Hara, A. Fukuoka, Appl. Catal. A: Gen. 409–410 (2011) 13–20.
[37] M. Yabushita, H. Kobayashi, A. Fukuoka, Appl. Catal. B: Environ. 145 (2014) 1–9.
[38] K. Chen, M. Tamura, Z.L. Yuan, Y. Nakagawa, K. Tomishige, ChemSusChem 6 (2013) 613–621.
[39] S. Liu, M. Tamura, Y. Nakagawa, K. Tomishige, ACS Sustain. Chem. Eng. 2 (2014) 1819–1827.
[40] Y. Nakagawa, Y. Shinmi, S. Koso, K. Tomishige, J. Catal. 272 (2010) 191–194.
[41] Y. Amada, Y. Shinmi, S. Koso, T. Kubota, Y. Nakagawa, K. Tomishige, Appl. Catal. B: Environ. 105 (2011) 117–127.
[42] K.Y. Chen, K. Mori, H. Watanabe, Y. Nakagawa, K. Tomishige, J. Catal. 294 (2012) 171–183.
[43] Y. Amada, H. Watanabe, Y. Hirai, Y. Kajikawa, Y. Nakagawa, K. Tomishige, ChemSusChem 5 (2012) 1991–1999.
[44] Y. Nakagawa, X. Ning, Y. Amada, K. Tomishige, Appl. Catal. A: Gen. 433-434 (2012) 128–134.
[45] Y. Amada, H. Watanabe, M. Tamura, Y. Nakagawa, K. Okumura, K. Tomishige, J. Phys. Chem. C 116 (2012) 23503–23514.
[46] Y. Nakagawa, K. Mori, K. Chen, Y. Amada, M. Tamura, K. Tomishige, Appl. Catal. A: Gen. 468 (2013) 418–425.
[47] M. Tamura, K. Tokonami, Y. Nakagawa, K. Tomishige, Chem. Commun. 49 (2013) 7034–7036.
[48] S. Liu, Y. Okuyama, M. Tamura, Y. Nakagawa, A. Imai, K. Tomishige, ChemSusChem 8 (2015) 628–635.
[49] S.R. Sashital, J.B. Cohen, R.L. Burwell Jr., J.B. Butt, J. Catal. 50 (1977) 479–493.
[50] J.W. Cook, D.E. Sayers, J. Appl. Phys. 52 (1981) 5024–5031.
[51] K. Okumura, J. Amano, N. Yasunobu, M. Niwa, J. Phys. Chem. B 104 (2000) 1050–1057.
[52] K. Okumura, S. Matsumoto, N. Nishiaki, M. Niwa, Appl. Catal. B: Environ. 40 (2003) 151–159.
[53] A.L. Ankudinov, B. Ravel, J.J. Rehr, S.D. Conradson, Phys. Rev. B 58 (1998) 7565–7576.
[54] K. Tomishige, K. Asakura, Y. Iwasawa, J. Catal. 149 (1994) 70–80.
[55] J. Yang, N. Li, S. Li, W. Wang, L. Li, A. Wang, X. Wang, Y. Cong, T. Zhang, Green Chem. 16 (2014) 4879–4884.
[56] R.R. Davda, J.W. Shabaker, G.W. Huber, R.D. Cortright, J.A. Dumesic, Appl. Catal. B: Environ. 43 (2003) 12–26.
[57] M. Tamura, Y. Amada, S. Liu, Z. Yuan, Y. Nakagawa, K. Tomishige, J. Mol. Catal. A: Chem. 388–389 (2014) 177–187.
[58] S. Liu, Y. Amada, M. Tamura, Y. Nakagawa, K. Tomishige, Catal. Sci. Technol. 4 (2014) 2535–2549.
[59] S. Liu, Y. Amada, M. Tamura, Y. Nakagawa, K. Tomishige, Green Chem. 16 (2014) 617–626.
[60] S. Kaneko, M. Izuka, A. Takahashi, M. Ohshima, H. Kurokawa, H. Miura, Appl. Catal. A: Gen. 427–428 (2012) 85–91.
[61] X. Hong, B. Li, Y.J. Wang, J.Q. Lu, G.S. Hu, M.F. Luo, Appl. Surf. Sci. 270 (2013) 388–394.

[62] H.-D. Kim, H.J. Park, T.-W. Kim, K.-E. Jeong, H.-J. Chae, S.-Y. Jeong, C.-H. Lee, C.-U. Kim, Catal. Today 185 (2012) 73–80.
[63] Y. Nakagawa, K. Takada, M. Tamura, K. Tomishige, ACS Catal. 4 (2014) 2718–2726.
[64] T. Ebashi, Y. Ishida, Y. Nakagawa, S.-i. Ito, T. Kubota, K. Tomishige, J. Phys. Chem. C 114 (2010) 6518–6526.
[65] Y. Ishida, T. Ebashi, S. Ito, T. Kubota, K. Kunimori, K. Tomishige, Chem. Commun. (2009) 5308–5310.
[66] M. Ronning, T. Gjervan, R. Prestivik, D.G. Nicholson, A. Holmen, J. Catal. 204 (2001) 292–304.
[67] Y. Shinmi, S. Koso, T. Kubota, Y. Nakagawa, K. Tomishige, Appl. Catal. B: Environ. 94 (2010) 318–326.
[68] A. Ciftci, D.A.J.M. Ligthart, A.O. Sen, A.J.F.V. Hoof, H. Friedrich, E.J.M. Hensen, J. Catal. 311 (2014) 88–101.